

Groundwater hydrogeochemistry in injection experiments simulating CO₂ leakage from geological storage reservoir



Qiang Yang^{a,*}, Juerg Matter^a, Martin Stute^{a,b}, Taro Takahashi^a, Gregory O'Mullan^{a,c}, Kelsey Umemoto^b, Kale Clauson^c, M. Elias Dueker^a, Natalia Zakharova^a, John Goddard^a, David Goldberg^a

^a Lamont-Doherty Earth Observatory, Columbia University, 61 Route 9W, Palisades, NY 10964, USA

^b Department of Environmental Science, Barnard College, 3009 Broadway, New York, NY 10027, USA

^c School of Earth and Environmental Sciences, Queens College of City University of New York, 65-30 Kissena Blvd., Flushing, NY 11367, USA

ARTICLE INFO

Article history:

Received 28 November 2013

Received in revised form 4 April 2014

Accepted 24 April 2014

Keywords:

Carbon dioxide geosequestration

Field injection

Mineral dissolution

Trace element release

Drinking water quality

ABSTRACT

Geologic carbon sequestration has the potential to reduce greenhouse gas concentrations in the atmosphere. However, one barrier to large scale implementation is concern for water quality degradation from leakage of high CO₂ fluids into drinking water aquifers. The hydrogeochemical response to simulated CO₂ leakage was studied to estimate major and trace element release and to develop criteria for water quality monitoring and risk assessment. In this study, approximately 3100 L aquifer water enhanced with 1 atmosphere pressure CO₂ gas was injected into a fracture zone located at 362–366 m below the ground surface in a sandstone/siltstone/mudstone interbedded aquifer in the Newark Basin. This was followed by a 3–6 week long incubation and then continuous monitoring of the hydrogeochemistry in the pumped-back water samples. Relative to background conditions, the recovered aquifer water displayed a decrease of pH, increase of alkalinity, Ca, Mg and Si concentrations, decrease of sulfate and Mo concentrations, and increased concentrations of trace elements including Fe, Mn, Cr, Co, Ni, Cu, Zn, Rb, Sr, Ba and U. These changes in aquifer water geochemistry can be explained by (a) dissolution of silicate and carbonate minerals and (b) trace element release that appear to be dependent on pH and pCO₂ and affected by the altered redox conditions in the aquifer. Rapid and simultaneous changes of pH, specific conductance, major and trace metal release in aquifer water could be used as indicators of CO₂ leakage from geologic sequestration sites. Hydrogeochemical parameters including pH, total dissolved solids and trace elements, particularly Fe, Mn, and Zn, need to be monitored in compliance with the U.S. Environmental Protection Agency (EPA) drinking water regulations.

© 2014 Elsevier Ltd. All rights reserved.

1. Introduction

Geologic sequestration of carbon dioxide (CO₂) into subsurface geologic formations has been considered as one of the most efficient short-term mitigation strategies to address environmental problems associated with anthropogenic CO₂ emissions to the atmosphere (IPCC, 2005). Safely sequestered CO₂ should take millions of years before reaching the surface because of the physical trapping mechanisms, e.g. confinement by low-permeable cap rocks and retention in pore space by capillary force, and the geochemical trapping by dissolution and mineralization (IPCC, 2005). However, the possible environmental impacts associated with the

upward migration of stored CO₂ through faults, fractures, poorly sealed or abandoned wells into shallow drinking water aquifers (Keating et al., 2013) have led to the slow process of public acceptance and the delay of wide applications of carbon capture and storage (CCS) (Bachu, 2008). The increased acidity from CO₂ intrusion into freshwater and altered aquifer redox conditions could enhance the dissolution of carbonate and silicate minerals, and increase the dissolved concentrations of trace elements (Kharaka et al., 2009; Little and Jackson, 2010; Lu et al., 2010; Peter et al., 2012; Romanak et al., 2012; Trautz et al., 2013; Yang et al., 2013; Zheng et al., 2012), which in turn has negative impacts on the groundwater quality (Lemieux, 2011).

Recent investigations into the impacts on shallow groundwater aquifers from CO₂ geosequestration, particularly under leakage scenarios, through laboratory incubation or leaching experiments and by geochemical model simulations have been well summarized

* Corresponding author. Tel.: +1 845 365 8629.

E-mail address: qyang@LDEO.columbia.edu (Q. Yang).

in Zheng et al. (2012). Field tests of CO₂ injection and observations of natural analogs have also been conducted recently. Matter et al. (2007) and Assayag et al. (2009) reported the decrease of pH, enrichment of major cations including dissolved inorganic carbon (DIC), Ca, Mg, K, and Na, and more rapid dissolution kinetics of carbonate minerals compared to silicate minerals during single-well push–pull experiments in an isolated and permeable interval at the contact zone of 250 m depth between the Palisades dolerite sill and underlying Newark Basin meta-sedimentary rocks (Assayag et al., 2009; Matter et al., 2007). Kharaka et al. (2010) observed rapid changes of pH, alkalinity, electrical conductance, major increases in the concentrations of Ca, Mg, Fe, Mn, Sr, Ba, Cd, Co, Cr, Zn, and detection of BTEX (benzene, toluene, ethylbenzene, and xylenes) in water samples collected from 1.5 m depth following a very shallow CO₂ injection at 2–2.3 m depth into a coarse sandy gravel alluvial deposit at the ZERT field site, Montana (Kharaka et al., 2010). Peter et al. (2012) reported an increase of total inorganic carbon, decrease of pH to 5.1, and the release of major cations including Ca, K, Mg and trace elements including Al, Si, Fe, Mn, Cu, Ni, Zn, Ba, Cd, Pb in shallow groundwater after a 10-day period CO₂ injection into a quaternary sand aquifer at 18 m below surface in northeast Germany (Peter et al., 2012). Trautz et al. (2013) observed a pH decrease of 3, and a pulse response of Ba, Ca, Cr, Sr, Mg, Mn and Fe in a controlled release field experiment in a fine-grained silty sand formation in southeastern Mississippi (Trautz et al., 2013). Yang et al. (2013) presented a single-well push–pull experiment in a shallow Gulf Coast aquifer in Cranfield, Mississippi and found enrichment of major ions including Ca, Mg, K, and Si, and trace elements (Yang et al., 2013). In contrast, Keating et al. (2010) observed minor effects of the relatively high levels of dissolved natural CO₂ on pH depression and trace element mobility due to the strong buffering capacity of the sandstone aquifer in New Mexico, while As, U and Pb are locally transported into the aquifer with CO₂-rich brackish water (Keating et al., 2010).

To date, these investigations on the hydrogeochemical processes and environmental impacts of simulated leakage or geogenic CO₂ are mostly limited in shallow sedimentary aquifers. While fractured bedrock formations often serve as drinking water aquifers, especially in rural areas, the environmental response to CO₂ leakage from geosequestration sites is rarely studied. It is also valuable to understand the subsurface hydrogeological and geochemical processes in fractured aquifer systems in response to elevated levels of CO₂ and compare with the finding in sedimentary aquifers. Groundwater flows preferentially through fractures in fractured bedrock formations, thus the residence time, reactive surface areas, impact zones of injected or leaked CO₂, as well as the geochemical conditions such as total dissolved solid, element concentration ranges and redox conditions, can be significantly different from those in sedimentary aquifers. Controlled injection of CO₂ into relatively deeper fractured bedrock aquifers to simulate CO₂ leakage from geosequestration therefore provides quantitative understanding of hydrogeochemical processes, spatial extent of impact zone, and environmental impacts associated with geologic carbon sequestration.

In this study, two field injection tests of aquifer water with elevated *p*CO₂ were conducted using single-well push–pull experiments in an isolated fracture zone at 362–366 m depth in a freshwater bedrock aquifer composed of sand and clay formations in the Newark Basin. The feasibility of carbon geosequestration has been studied previously in the Newark Basin (Assayag et al., 2009; Icenhower et al., 2013; Matter et al., 2007; McGrail et al., 2006). The main objectives of this study included: (1) quantifying the changes in elemental composition of aquifer water, relative to background conditions, following the injection of high *p*CO₂ fluid; (2) estimating the release rates of major and trace elements as a function of *p*CO₂; and (3) evaluating the degradation of water quality, relative to the

U.S. Environmental Protection Agency (EPA) Maximum Contaminant Levels (MCLs) for drinking water. In addition, the results from these experiments can provide valuable insight into developing criteria for diagnostic monitoring of CO₂ leakage.

2. Materials and method

2.1. Study site

The Newark Basin is located mainly in northern New Jersey and stretches into southeastern Pennsylvania and southern New York. It is a lacustrine sediment-filled rift basin formed 200 million years ago in the Late Triassic and intruded later by the Palisades dolerite sill in the Early Jurassic. The sedimentary formations are up to 3350 m thick and contain characteristic red bed sediments due to the abundant iron oxide minerals. Interbedded layers with various grain sizes range from sandstone, siltstone, to mudstone (Olsen et al., 1996).

The test well (41°00′14.4″ N, 73°54′45.5″ W, well head elevation 117 m a.s.l.), a borehole drilled to a total depth of 457 m, is located at the Lamont-Doherty Earth Observatory (LDEO) in Palisades, New York. At this site, the Palisades dolerite sill is 230 m thick from the land surface with a few meters of overburden at the top and underlain by metamorphosed sedimentary rocks of the Pas-saic Formation (Burgdorff and Goldberg, 2001; Matter et al., 2006). Previous hydrogeological testing has identified three major permeable zones, including a shallow zone (230–240 m below the ground surface) at the contact between the Palisades dolerite sill and sedimentary formations with a transmissivity of 0.092 m²/day, another zone at 300 m depth within sedimentary formations with an estimated transmissivity of 0.86 m²/day, and a deep zone at 364 m depth within sedimentary formations with a very low transmissivity of 0.023 m²/day and a non-detectable ambient flow rate. The deepest zone with the lowest transmissivity is used in this study to minimize the risk of losing injected solution and thus to allow a longer incubation with elevated concentration of CO₂. This zone does not exhibit apparent fractures in the borehole wall images according to the geophysical logs, but the water level drawdown and recovery data during the pumping tests suggest this tested zone is likely characterized by a combination of primary porosity (porous media of tight sandstone type) and secondary porosity (fracture system) (Unpublished results).

2.2. Field injection tests

The first of the two single-well push–pull experiments was conducted in the 362–366 m interval of the TW-3 test well during summer 2011.

2.2.1. Background characterization phase

Prior to injection, a pumping test at a flow rate of ~3.5 L/min from this interval, sealed by inflatable packers, was performed for approximately one week to estimate the interval transmissivity. Fresh fracture water samples representative of the targeted interval were collected after the monitored water geochemical parameters, including pH, specific conductance (SC), oxidation-reduction potential (ORP or redox potential) and dissolved oxygen (DO) levels were stabilized to characterize background conditions.

2.2.2. Push/injection phase

Approximately 3400 L of this fresh fracture water was collected and then saturated with 1 atmosphere pressure of CO₂ (*p*CO₂) by slowly bubbling pure CO₂ gas for 16 h under the ambient barometric pressure in three sterilized polyethylene storage tanks at the well site. Bromide (as KBr) was mixed into the water at an average concentration of 45.53 mg/L and used as a conservative ionic

tracer to understand the hydrogeological flow and mixing processes during the push–pull experiment. A total of 3060 L of this treated aquifer water was injected back into the aquifer for 11.1 h at a flow rate of approximately 4.6 L/min, while the CO₂ bubbling continued during the injection to ensure constant 1 atmosphere pCO₂. As the CO₂-treated water was injected, SF₆, a second conservative tracer in dissolved gaseous phase, was dynamically introduced into the injection tube using a HPLC pump (Cole Palmer Series I, Vernon Hills, IL) at a rate of 0.4 ml SF₆-saturated water per minute at a constant temperature of 0 °C. Approximately 70 L of untreated aquifer water with an ambient CO₂ level (134–136 μatm pCO₂) and without tracers was injected afterwards as a chaser solution to push the injected 1 atmosphere pCO₂ water into the aquifer layer.

2.2.3. Incubation phase

An incubation period of 20 days, with the injection interval sealed by inflatable packers, allowed enough time for the injected fluid to react with aquifer materials and to also ensure an appropriate recovery of injected fluid by avoiding the solute loss due to long-term mixing, dilution and biogeochemical reactions. Test samples were collected 7 days after the injection to check the tracer concentrations and hydrogeochemical parameters such as pH, SC and ORP. The test sampling volume was minimized to 400 L (13% of the volume of injected water) to keep the disturbance as small as possible.

2.2.4. Pull/extraction phase

After the incubation period, the interval was pumped continuously at 2.6 L/min for 33 days for a total of 123,550 L, about 40 times of the injected water. A YSI multi-parameter meter with a flow through cell was used to monitor temperature, pH, SC, ORP and DO concentrations continuously throughout the pumping back. A total of 20 sets of discrete samples were collected during this recovery phase. The samples were divided into three groups for comparison purpose, (1) early extraction: samples collected on the first day of continuous pumping when the extracted volume (V-extracted) was less than the injected volume (V-injected); (2) mid extraction: samples collected when 1 < V-extracted/V-injected < 10; (3) late extraction: samples collected when V-extracted/V-injected > 10.

This push–pull experiment was repeated in the same interval during summer 2012. Approximately 3090 L of aquifer water saturated with 1 atm pCO₂ was injected at a rate of 5.1 L/min for 10 h and then incubated for 40 days. Continuous pumping at a flow rate of 1.7 L/min was followed for 30 days with a total volume of about 25 times of the injected water during the extraction phase.

2.3. Sample collection and analysis

Each set of groundwater samples included five aliquots. The first aliquot was filtered through 0.45 μm membrane filter for the analysis of major anions including alkalinity, the second aliquot was also filtered through 0.45 μm membrane filter and then acidified to 1% HNO₃ (Fisher Optima) for the analysis of major cations and trace elements, the third aliquot was the unfiltered water sample for Br[−] tracer analysis, the fourth aliquot was the unfiltered water sample collected using air-tight syringes for total CO₂ (tCO₂) and pCO₂ analyses, and the fifth aliquot was collected in evacuated serum bottles with head space for SF₆ tracer analysis.

Major anions, including fluoride, chloride, nitrate, nitrite, phosphate, sulfate, and bromide (tracer), were measured by Ion Chromatography (IC) following the U.S. EPA method 300.0. The concentrations of major cations and trace elements were measured by High-Resolution Inductively Coupled Plasma Mass Spectrometry (HR ICP-MS) following a revised EPA method 200.8 (Cheng et al., 2004). NIST standard reference material 1643E “trace elements in

water” and an internal artificial groundwater “LDEO” were used for QA/QC standards. All the elemental concentrations reported in this research agree within ±10% of the reference values. The total CO₂ was analyzed using a coulometer method at LDEO (Chipman et al., 1993) with a precision of about ±0.5%, and was calibrated using the CO₂ reference solutions provided by A. G. Dickson of the Scripps Institution of Oceanography (Dickson, 2001). The pCO₂ in the water samples was measured by a gas–water equilibration method in a closed recirculation system (Chipman et al., 1993) using a CO₂/H₂O Analyzer (LI-COR LI-840) with a precision of about ±1%. The CO₂ analyzer was calibrated with four standard CO₂–air mixtures, of which CO₂ concentrations were traceable to the World Meteorological Organization (WMO) standards for atmospheric research. SF₆ concentrations in the head space were measured using Gas Chromatography (SRI 8610 C) at LDEO with a precision of about ±2%, and the concentrations in the water samples were calculated based on the volume of head space and the solubility. Alkalinity was measured by titration to the end point of pH 4.5 using H₂SO₄ of known concentrations with a precision of about ±2%.

2.4. Drill cuttings from the injection interval

A drill cutting sample collected at 365 m depth when the borehole was drilled, was completely dissolved with a mixture of concentrated HF and HNO₃ in a microwave digestion system (Milestone ETHOS EZ), and the concentrations of major and trace elements were determined at a precision of about ±5% using a HR ICP-MS (Cheng et al., 2004) following the EPA method 3052. The mineral composition of the drill cutting sample was reconstructed based on the chemical composition using the MINLITH program (Rosen et al., 2004).

2.5. Tracer mixing ratio

The mixing ratio (X_{mix}), which is the fraction of the injected water in each extracted water sample, was estimated using the concentrations of the non-reactive tracers (KBr and SF₆):

$$X_{\text{mix}} = \frac{C_{\text{tracer(extracted)}} - C_{\text{tracer(background)}}}{C_{\text{tracer(injected)}} - C_{\text{tracer(background)}}} \quad (1)$$

where $C_{\text{tracer(extracted)}}$ is the concentration of tracer in extracted water samples, $C_{\text{tracer(injected)}}$ is the tracer concentration in the injected water, and $C_{\text{tracer(background)}}$ is the background concentrations of tracers in the aquifer (very low, see Tables 2 and 3).

This ratio was used to calculate the concentration of a specific solute (C_{mix}) if based solely on the mixing of background water and injected solution:

$$C_{\text{mix}} = X_{\text{mix}}C_{\text{injected}} + (1 - X_{\text{mix}})C_{\text{background}} \quad (2)$$

where C_{injected} and $C_{\text{background}}$ are concentrations of the specific solute in injected solution and background aquifer water, respectively.

Breakthrough curves of hydrogeochemical tracers during the extraction phase were plotted as the tracer mixing ratio vs. V-extracted/V-injected. Bromide and SF₆ breakthrough curves were also used to calculate the recovery percentage (the total extracted mass/injected mass in percentage) as they were considered conservative tracers.

2.6. Elemental release rate

As the acidified water was injected into the aquifer layer, the advancing injected plume was mixed with the background aquifer water, and the mixing ratio of injected solution was decreased from the well head to the plume front. In the early stage of incubation, the remaining hydraulic pressure could extend the area of

the plume front, while it is assumed that during the incubation period the majority of injected water stayed in place without significant lateral and vertical transport. As the water was pumped back, the mixing ratio of injected solution in the collected samples decreased, and the water samples collected during the later stages of extraction exhibited higher degree of mixing with background aquifer water than those collected during the earlier stages. Thus, we consider that a parcel of injected water diluted with the aquifer water reacted with the surrounding rocks for the duration of incubation until the sampling point. Changes observed in the collected water samples reflect the chemical reactions occurred during the incubation period, and may be defined as $(C_{\text{measured}} - C_{\text{mix}})$, where C_{measured} is the measured concentration of a specific solute in a specific water sample and used as the end-point concentration, C_{mix} is the concentration based solely on the mixing and used as the start-point concentration. The mean release rate is approximated by dividing the change by the total reaction time and normalized by the reactive surface area:

$$R = \frac{(C_{\text{measured}} - C_{\text{mix}})V_{\text{reacted}}/A_{\text{reactive}}}{t_{\text{reaction}}} \quad (3)$$

where R is the release rate, V_{reacted} is the volume of reacted water, A_{reactive} is the reactive surface area, and t_{reaction} is the time elapsed since the end of injection.

A_{reactive} was estimated using the mass of impacted aquifer and the specific surface area:

$$A_{\text{reactive}} = \left(\frac{V_{\text{reacted}}}{n_e} \right) \rho SA_s \quad (4)$$

where n_e is the effective porosity of 0.03 from the best estimate of field hydrophysical logging, and hence (V_{reacted}/n_e) is the volume of the rocks that hosted the volume of the water involved in chemical reactions. ρ is the average bulk rock density of 2.67 g/cm³ measured from core samples from various sedimentary formations in the Newark Basin, SA_s is the specific surface area of 4 m²/g estimated from BET measurements of sediment samples from the Newark Basin. It is assumed that the surface area measured by BET represents the area for chemical reactions.

Combining Eqs. (3) and (4), the calculation of elemental release rates can be simplified as,

$$R = (C_{\text{measured}} - C_{\text{mix}})n_e/\rho/SA_s/t_{\text{reaction}} \quad (5)$$

This equation is used for the rates shown in Fig. 6.

2.7. Statistical analysis

Correlation coefficients (R) between parameters were calculated to measure the strength and direction of the linear relationship between two variables. Two-tailed Student's t -test (p value) is used to determine if two sets of data are statistically significantly different from each other, with smaller values indicating more distinct difference. Due to the environmental sensitivity of leakage detection and the associated changes to potential drinking water sources, p values less than 0.1, rather than a more commonly used level of 0.05, are considered to indicate a significant difference in this study. This more precautionary approach provides a more conservative basis for detecting altered conditions in the aquifers.

3. Results

3.1. Composition of sediment from the injection interval

Results from the digestion experiment (Table 1) showed a very high mass percentage of SiO₂ (91%) and low concentrations of Al, Ca, Mg, Na, and Fe in the drill cutting sample collected from the injection interval. The mineral composition estimated using the

Table 1

Chemical composition (a) and calculated mineral composition* (b) of drill cuttings from the injection interval at TW-3.

(a)					
	wt%	Trace element	mg/kg	Trace element	mg/kg
SiO ₂	90.95	Li	6.2	Zn	1.1
Al ₂ O ₃	3.93	Be	0.3	As	0.4
CaO	0.60	S	13.1	Sr	37.9
MgO	0.05	V	3.5	Zr	48.0
Na ₂ O	0.18	Cr	4.4	Cs	2.0
K ₂ O	3.20	Mn	12.6	Ba	498.4
Fe ₂ O ₃	0.06	Co	3.0	Pb	7.9
P ₂ O ₅	0.03	Ni	1.2	U	0.5
TiO ₂	0.03	Cu	3.3		

(b)	
Mineral	wt %
Quartz	77.9
Orthoclase	18.7
Plagioclase	1.69
Calcite	0.80
Dolomite	0.18
Ankerite	0.12
Illite	0.49
Apatite	0.07
Rutile	0.03

* Mineral composition calculated using MINLITH (Rosen et al., 2004).

MINLITH program showed very high weight percentages of quartz (78%), orthoclase (19%) and plagioclase (1.7%), low percentages of calcite (0.8%), dolomite (0.18%), illite (0.49%), and very low portions of ankerite (0.12%), apatite (0.07%), and rutile (0.03%). This suggests a high content of quartz and feldspar but low concentrations of carbonate and clay minerals in the injected interval of the aquifer, although the possible loss of fine grained sediments and some heavy minerals during drilling processes cannot be ruled out, which could contain higher levels of clay minerals and trace elements.

3.2. Tracer breakthrough curves

During both injection experiments, the fraction of bromide and SF₆ decreased rapidly from 50–70% at the beginning of the extraction phase to less than 10% when 1.5 times of the injected volume was extracted, and then to less than 1% when 10 injection volumes were extracted, followed by a long tail (Fig. 1). Bromide concentrations in the aquifer were observed higher than 1‰ of the injected solution even after 37.4 and 24.5 times of the injected volume were extracted in 2011 and 2012 experiments, respectively. The rapid decrease in the early extraction phase and the long tail in the late

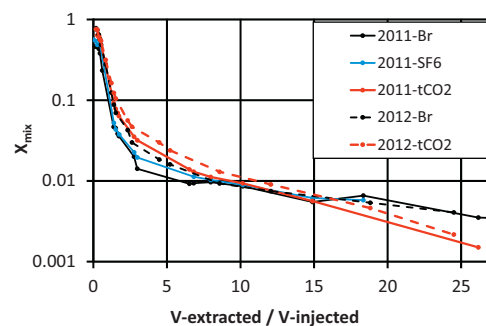


Fig. 1. The breakthrough curves of bromide, SF₆ and total CO₂ in the TW-3 push-pull experiments. $X_{\text{mix}} = (C_{\text{tracer(extracted)}} - C_{\text{tracer(background)}}) / (C_{\text{tracer(injected)}} - C_{\text{tracer(background)}})$

phase suggest a dual-porosity system containing both highly transmissive fractures and low-permeability fine grained sediments.

3.3. Hydrogeochemical parameters and $t\text{CO}_2$, $p\text{CO}_2$

In 2011, prior to injection, the background fracture water had a slightly alkaline pH of 8.2 and a specific conductance of $1300 \mu\text{S}/\text{cm}$ (Table 2). The low DO ($0.6 \text{ mg}/\text{L}$ or $20 \mu\text{mol}/\text{L}$, 6% of the atmospheric saturation concentration) and low ORP ($58\text{--}71 \text{ mV}$) indicated a sub-oxic condition. Total CO_2 was $0.87 \text{ mmol}/\text{L}$ in the background water, with the $p\text{CO}_2$ of $134\text{--}136 \mu\text{atm}$.

After the water was treated with one atmosphere CO_2 , the injected water had an average pH of 4.38 and an average ORP of 316 mV . The total CO_2 increased to $33.90 \text{ mmol}/\text{L}$, with an estimated $p\text{CO}_2$ of 0.90 atm , indicating near saturation of CO_2 . The dissolution of CO_2 and introduction of KBr tracer increased the specific conductance to $1447 \mu\text{S}/\text{cm}$.

After 7 days (161 h) incubation, the water collected during test sampling showed a buffered pH of 6.05 and an increased specific conductance to $1728 \mu\text{S}/\text{cm}$, which indicated the quick dissolution of aquifer materials. A very low ORP (-266 mV) and depleted DO ($0.15 \text{ mg}/\text{L}$ or $5 \mu\text{mol}/\text{L}$, 1.5% of the atmospheric saturation concentration) indicated a strong reducing environment. The measured total CO_2 of $24.45 \text{ mmol}/\text{L}$ was higher than the total CO_2 of $16.14 \text{ mmol}/\text{L}$ based solely on the mixing process, indicating the introduction of carbon species from the aquifer. The $p\text{CO}_2$ of 0.287 atm was lower than 0.416 atm estimated from a simple mixing, which suggests an increase in pH and alkalinity by the dissolution of minerals.

During the continuous extraction phase, pH increased rapidly in the first few days and then followed by a gradual increase to 7.91 after 33 days. ORP rapidly increased to $\sim 0 \text{ mV}$ during the early extraction phase when 0.6 times of injected volume was pumped, and then showed fluctuation between -44 and $+47 \text{ mV}$ during the mid and late extraction phases. Total CO_2 decreased to the background levels at the end of extraction phase, while the $p\text{CO}_2$ at the end of extraction ($356 \mu\text{atm}$) was still higher than the background levels ($134\text{--}136 \mu\text{atm}$).

In 2012, slightly higher pH (8.54), DO ($1.3 \text{ mg}/\text{L}$ or $40 \mu\text{mol}/\text{L}$, 12% of the atmospheric saturation concentration) and ORP ($74\text{--}84 \text{ mV}$), and a lower specific conductance ($754 \mu\text{S}/\text{cm}$) were observed in the background fracture water from the same interval prior to injection (Table 3). Similar trends of groundwater geochemistry in response to CO_2 injection were observed, except the ORP in the injection interval did not drop as significantly as it did in 2011, which may be related to the higher DO of the ambient groundwater in 2012.

3.4. Major ions

In both experiments, the background aquifer water prior to CO_2 injection showed a Na-SO_4 water type. When the aquifer water was bubbled with CO_2 in the storage tanks, its major ion concentrations, including alkalinity, were virtually unchanged (except K due to the introduction of KBr as a tracer), but its total CO_2 increased dramatically, which indicated the CO_2 was mainly in the dissolved gas phase (Tables 2 and 3).

After the incubation periods during the 2011 and 2012 experiments, the water samples collected during the early extraction phase showed a water chemistry change to Ca-HCO_3 type, due to the large increase of HCO_3^- and Ca^{2+} . Alkalinity, Ca, Mg and Si concentrations increased to $7.9\text{--}11.9$, $3.0\text{--}5.2$, $1.8\text{--}3.5$, and $1.8\text{--}2.1$ times of background levels (Figs. 2A and 3A), respectively. Sulfate concentrations showed a maximum decrease of 20–30% in the early extraction phase after incubation.

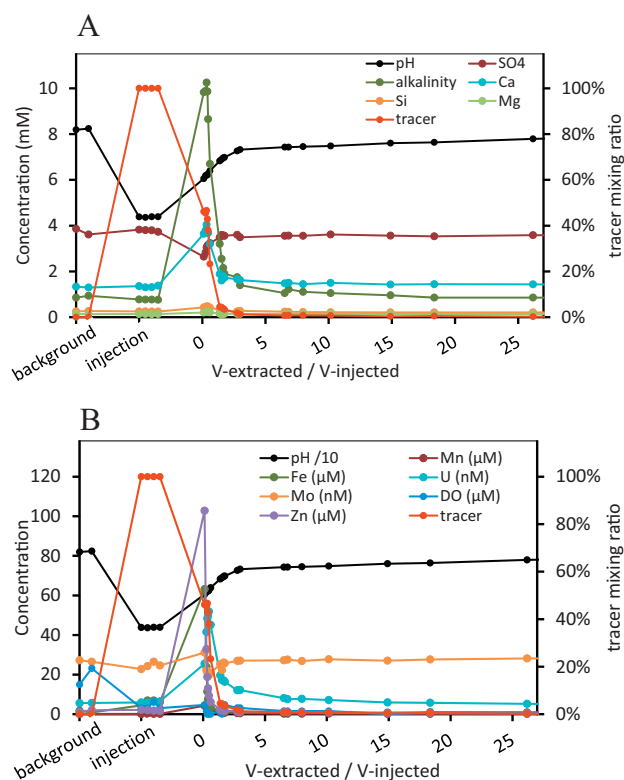


Fig. 2. Concentrations of selected major ions (A) and trace elements (B) in background, injected, and extracted solutions during 2011 push-pull experiment in TW-3 well.

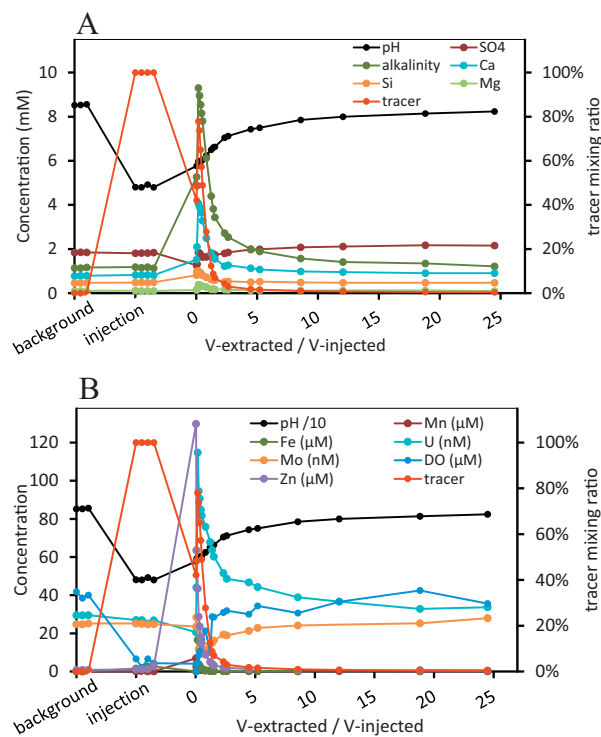


Fig. 3. Concentrations of selected major ions (A) and trace elements (B) in background, injected, and extracted solutions during 2012 push-pull experiment in TW-3 well.

Table 2
Groundwater hydrogeochemistry in the 2011 push–pull field experiment.

experiment stage	sample ID	time since injection hour	V _{pumped} /V _{injected}	Temperature °C	pH	Specific Conductance $\mu\text{S/cm}$	DO mg/L	ORP mv	Br mg/L	mixing ratio	SF ₆ pptv	TCO ₂ mM	ρCO_2 μatm	Na mM	Mg mM	K mM	Ca mM	Si mM	Cl ⁻ mM	SO ₄ ²⁻ mM	alkalinity mM		
background	TW3-100			15.0	8.19	1335	0.48	58	0.49	0%		0.87	136	6.65	0.14	0.02	1.33	0.26	3.22	3.86	0.86		
	TW3-101			17.9	8.24	1267	0.74	71	0.37	0%	1	0.87	134	7.01	0.13	0.03	1.30	0.27	3.10	3.62	0.94		
injection	TW3-102			19.6	4.38	1443	0.10	320	44.76	100%	31800	33.90	900000	6.64	0.14	0.39	1.36	0.26	3.38	3.83	0.78		
	TW3-103			22.0	4.36	1448	0.10	307	45.33	100%				6.83	0.14	0.38	1.30	0.25	3.39	3.80	ND		
	TW3-104			23.7	4.39	1450	0.20	322	46.09	100%				6.82	0.13	0.37	1.31	0.25	3.39	3.79	ND		
	TW3-105								45.94	100%				6.49	0.14	0.36	1.38	0.25	3.34	3.73	0.76		
	TW3-106	161	0.11	15.6	6.05	1728	0.15	-266	21.24	46.2%	17400	24.45	287000	6.57	0.21	0.22	3.64	0.43	2.63	2.65	9.82		
early extraction	TW3-107	476	0.26	16.8	6.18	1861	0.05	-229	20.91	45.4%	15400	21.91	254000	6.37	0.22	0.17	3.78	0.44	2.78	2.82	9.88		
	TW3-108	477	0.34	16.7	6.20	1910	0.00	-151	21.45	46.6%		22.47	254000	6.99	0.25	0.17	4.04	0.47	2.89	3.04	10.25		
	TW3-109	478	0.40	16.7	6.22	1896	0.00	-88	19.77	42.9%	17600	21.33	235000	7.10	0.23	0.16	3.72	0.47	2.92	3.11	9.86		
	TW3-110	479	0.46	15.9	6.26	1864	0.00	-58	17.57	38.0%		19.57	202000	7.57	0.23	0.14	3.68	0.46	2.91	3.15	8.65		
	TW3-111	482	0.60	15.3	6.39	1741	0.00	3	10.94	23.3%				7.40	0.22	0.10	3.20	0.42	2.85	3.24	6.70		
mid extraction	TW3-112	496	1.38	18.6	6.83	1472	0.05	-19	2.48	4.5%	1660	3.88	16700	7.15	0.15	0.05	1.89	0.32	2.91	3.48	3.20		
	TW3-113	498	1.52	19.4	6.89	1462	0.00	24	2.41	4.4%	1380	3.45	13300	6.13	0.13	0.04	1.60	0.25	3.03	3.59	2.55		
	TW3-114	501	1.65	17.1	6.96	1447	0.15	17	2.11	3.7%		3.15	10400	7.35	0.15	0.05	1.80	0.29	3.01	3.57	2.15		
	TW3-115	502	1.74	16.5	6.98	1442	0.15	47	1.99	3.5%	1200	2.97	9300	6.54	0.15	0.04	1.72	0.27	3.00	3.56	1.90		
	TW3-116	521	2.76	18.5	7.26	1412	0.10	7	1.27	1.9%	719	2.02	3620	7.32	0.15	0.03	1.66	0.26	3.01	3.60	1.75		
	TW3-117	525	2.99	17.5	7.32	1412	0.10	-13	1.01	1.3%	621	1.91	2980	7.52	0.15	0.04	1.62	0.28	2.88	3.49	1.40		
	TW3-118	593	6.52	19.3	7.43	1402	0.05	-35	0.79	0.8%		1.32	1640	6.91	0.14	0.03	1.48	0.24	2.94	3.55	1.05		
	TW3-119	598	6.82	16.8	7.43	1399	0.05	-25	0.79	0.8%	358	1.29	1570	7.33	0.14	0.03	1.50	0.23	2.94	3.56	1.22		
	TW3-120	621	7.98	17.2	7.45	1397	0.05	-44	0.80	0.8%	327	1.23	1440	7.04	0.14	0.03	1.44	0.22	2.94	3.56	1.11		
	late extraction	TW3-121	664	10.15	18.4	7.48	1413	0.05	-12	0.76	0.7%	284	1.17	1290	7.11	0.15	0.03	1.50	0.22	2.96	3.62	1.06	
		TW3-122	760	14.89	19.4	7.60	1409	0.00	21	0.62	0.4%	195	1.05	892	7.06	0.14	0.03	1.43	0.21	2.91	3.57	0.96	
		TW3-123	832	18.35	19.2	7.64	1406	0.03	28	0.67	0.5%				7.17	0.14	0.03	1.44	0.21	2.88	3.53	0.86	
TW3-124		1000	26.17	18.3	7.79	1402	0.03	15	0.53	0.2%		0.91	500	7.27	0.14	0.03	1.44	0.22	2.91	3.59	0.86		
TW3-125		1264	37.27	19.8	7.92	1395	0.02	13	0.51	0.2%				7.27	0.14	0.03	1.39	0.21	2.87	3.55	0.82		
TW3-126		1266	37.36	20.0	7.91	1395	0.02	3	0.51	0.2%		0.85	358	7.23	0.14	0.03	1.38	0.21	2.85	3.53	0.82		
EPA secondary MCL					6.5–8.5	780*																7.05	2.60

* estimated based on the secondary MCL of 500 mg/L for TDS.

experiment stage	sample ID	Li μM	Be nM	Cr nM	Mn μM	Fe μM	Co nM	Ni μM	Cu μM	Zn μM	As nM	Se nM	Rb nM	Sr μM	Zr nM	Mo nM	Cd nM	Sb nM	Cs nM	Ba nM	Ti nM	Pb nM	U nM
background	TW3-100	4.7	7	3	0.16	1.77	2.26	0.26	0.07	1.3	19	10	30	13	2.9	27	1.0	0.3	1.6	75	3.0	5.4	5.6
	TW3-101	4.7	5	3	0.12	0.89	1.19	0.27	0.06	2.0	21	12	30	12	2.2	27	0.9	0.2	1.5	66	2.9	1.8	5.7
injection	TW3-102	4.7	5	7	0.17	4.48	1.83	0.30	0.17	2.2	17	11	35	13	2.1	23	43.5	0.7	1.5	74	5.9	54.6	5.9
	TW3-103	4.7	6	9	0.20	6.87	2.04	0.36	0.17	2.0	19	12	34	13	1.9	24	62.3	0.8	1.4	70	5.1	53.8	5.9
	TW3-104	4.7	5	22	0.21	6.91	2.37	0.34	0.19	1.7	15	10	35	13	3.2	26	58.9	0.8	1.4	73	4.4	57.8	6.3
	TW3-105	4.5	5	9	0.18	6.16	1.96	0.31	0.18	1.6	17	9	34	13	2.3	25	41.5	0.8	1.4	77	4.3	45.4	6.5
incubation (test sampling)	TW3-106	4.3	21	11	4.32	63.14	13.74	0.44	0.96	102.8	13	8	67	19	4.6	31	2.5	1.1	1.6	263	2.8	5.2	25.5
early extraction	TW3-107	4.4	17	15	3.58	23.83	7.80	0.37	0.07	32.8	13	7	67	21	4.8	22	2.0	0.6	1.7	218	2.9	5.0	41.5
	TW3-108	4.7	20	9	3.31	11.41	5.99	0.34	0.07	18.8	13	9	69	23	5.3	21	1.9	0.6	1.8	206	2.9	4.4	48.4
	TW3-109	4.7	19	10	3.01	7.58	4.65	0.30	0.09	13.0	14	6	67	22	4.2	20	1.9	0.6	1.7	191	2.8	4.7	49.9
	TW3-110	4.8	18	7	2.74	5.22	3.85	0.30	0.12	9.4	12	6	66	22	4.1	20	1.4	0.5	1.7	179	2.5	4.1	51.9
	TW3-111	4.8	13	5	2.08	3.48	3.50	0.29	0.17	6.1	13	7	57	21	3.9	21	1.6	0.7	1.6	150	2.3	4.1	45.1
mid extraction	TW3-112	4.9	7	3	0.85	1.58	2.29	0.27	0.09	2.2	13	6	37	15	2.7	25	1.0	0.3	1.4	92	1.9	2.9	19.6
	TW3-113	4.2	5	2	0.67	1.23	2.10	0.28	0.09	1.9	11	7	36	13	3.0	22	0.9	0.3	1.3	88	2.1	2.5	17.2
	TW3-114	4.8	7	2	0.75	1.40	2.01	0.29	0.09	1.8	12	10	35	15	2.4	26	1.0	0.3	1.4	86	1.9	2.6	17.0
	TW3-115	4.6	5	3	0.70	1.25	2.08	0.29	0.08	1.8	11	8	35	14	2.7	26	1.0	1.5	1.4	87	1.9	2.8	16.4
	TW3-116	4.8	4	2	0.55	1.75	1.79	0.26	0.07	1.2	10	8	34	14	2.2	27	1.0	0.3	1.4	76	1.7	2.4	12.1
	TW3-117	5.0	4	2	0.48	0.86	1.65	0.27	0.07	1.2	13	10	31	14	2.4	27	0.8	0.3	1.3	78	1.9	2.6	12.2
	TW3-118	4.9	4	2	0.34	0.87	1.95	0.27	0.06	1.2	14	6	31	14	2.7	27	1.1	0.2	1.3	71	1.8	2.5	8.1
	TW3-119	4.9	4	2	0.32	0.85	1.63	0.28	0.06	1.1	12	7	31	13	2.3	28	0.9	0.3	1.3	70	1.6	2.0	7.6
late extraction	TW3-120	4.7	NA	3	0.32	1.01	2.23	0.26	0.06	1.0	14	NA	29	13	2.8	27	0.4	0.2	2.5	72	2.0	1.3	7.8
	TW3-121	5.0	NA	4	0.29	0.93	2.32	0.27	0.05	0.8	12	NA	29	13	2.6	28	0.4	0.2	2.0	71	2.1	1.2	7.2
	TW3-122	4.9	NA	1	0.24	0.79	2.04	0.30	0.05	0.6	15	NA	28	13	2.4	27	0.3	0.2	1.7	68	1.9	1.2	6.0
	TW3-123	5.0	NA	3	0.23	1.02	2.11	0.27	0.06	0.6	15	NA	27	13	2.6	28	0.4	0.5	1.5	87	1.8	3.0	5.7
	TW3-124	5.0	NA	2	0.20	0.87	1.88	0.26	0.05	0.4	16	NA	26	14	2.5	28	0.4	0.2	1.5	62	1.7	1.1	5.3
	TW3-125	5.1	NA	2	0.18	0.79	1.86	0.28	0.05	0.3	15	NA	24	14	2.3	28	0.3	0.2	1.4	58	1.4	1.0	4.8
	T																						

Table 3
Groundwater hydrogeochemistry in the 2012 push–pull field experiment.

experiment stage	sample ID	time since injection hour	$V_{pumped}/V_{injected}$	Temperature °C	pH	Specific Conductance $\mu\text{S/cm}$	DO mg/L	ORP mv	Br mg/L	mixing ratio	TCO_2 mM	ρCO_2 μatm	Na mM	Mg mM	K mM	Ca mM	Si mM	Cl ⁻ mM	SO_4^{2-} mM	alkalinity mM
background	TW3-202			17.4	8.52	762	1.34	74	0.00	0%	1.10	106	6.31	0.10	0.03	0.78	0.46	2.33	1.84	1.14
	TW3-203			18.3	8.53	744	1.23	74	0.00	0%			6.23	0.10	0.03	0.79	0.46	2.33	1.85	1.14
	TW3-204			15.9	8.56	756	1.28	84	0.00	0%			6.38	0.11	0.03	0.79	0.47	2.37	1.85	1.17
in tank	tank-1				4.64			0.10					5.95	0.11		0.78	0.45	2.38	1.86	1.14
	tank-2				4.66			0.10	86.21				6.29	0.11	1.05	0.82	0.46	2.39	1.82	1.17
	tank-3				4.66			0.15	86.34				6.28	0.11	1.05	0.80	0.46	2.37	1.83	1.16
injection	TW3-205			20.4	4.81	920	0.21	325	88.87	100%	39.12	970608	6.34	0.12	1.02	0.83	0.48	2.36	1.81	1.18
	TW3-206			21.4	4.80	925	0.07	328	90.01	100%	35.02	894204	6.44	0.11	1.16	0.83	0.49	2.36	1.82	1.15
	TW3-207			24.4	4.92	928	0.21	334	88.46	100%	33.28	906979	6.43	0.10	1.19	0.83	0.47	2.37	1.81	1.18
	TW3-208			22.4	4.80	903	0.14	340	76.26	100%	36.18	949358	6.63	0.10	1.05	0.81	0.49	2.35	1.84	1.13
incubation (test sampling)	TW3-209	239	0.03	19.1	5.77	1028	0.13	43	36.16	42.1%	9.54	168589	5.02	0.14	0.46	1.52	0.81	2.29	1.26	5.27
	TW3-210	241	0.06						41.66	48.5%	18.00	318060	6.09	0.18	0.74	2.10	0.99	2.33	1.33	4.88
early extraction	TW3-211	955	0.18	21.3	5.98	1374	0.14	70	66.94	77.9%	27.51	429697	8.14	0.39	1.15	4.07	1.01	2.61	1.84	9.30
	TW3-212	957	0.27	20.8	5.91	1357	0.27	132	63.37	73.8%	27.13	447020	8.04	0.37	0.94	3.92	0.93	2.60	1.82	8.96
	TW3-213	959	0.35	18.6	5.99	1314	0.34	134	55.85	65.0%	22.36	327597	7.95	0.35	0.75	3.80	0.92	2.56	1.73	8.54
	TW3-214	961	0.44	17.6	6.01	1248	0.48	142	49.18	57.2%	20.77	292460	7.82	0.32	0.64	3.64	0.86	2.53	1.67	8.16
	TW3-215	962	0.51	17.6	6.05	1218	0.53	144	42.04	48.9%	19.97	270490	7.48	0.31	0.55	3.29	0.81	2.51	1.64	7.80
mid extraction	TW3-216	970	0.83	16.6	6.24	1069	0.68	149	23.86	27.8%	12.11	130041	7.06	0.28	0.33	2.50	0.72	2.50	1.65	6.12
	TW3-217	978	1.22	17.7	6.50	931	0.32	128	10.66	12.4%	6.76	51260	6.58	0.17	0.21	1.82	0.62	2.52	1.69	4.40
	TW3-218	982	1.40	16.5	6.60	890	0.92	140	7.53	8.8%	5.37	33969	6.40	0.19	0.19	1.65	0.60	2.54	1.78	3.82
	TW3-219	985	1.53	17.4	6.63	883	0.91	134	5.97	7.0%	4.73	28819	6.43	0.17	0.16	1.56	0.59	2.54	1.74	3.44
	TW3-220	1003	2.33	15.5	7.05	817	0.99	115	3.67	4.3%	3.04	8183	5.88	0.17	0.10	1.23	0.52	2.56	1.81	2.72
	TW3-221	1009	2.62	15.0	7.12	809	1.02	106	2.57	3.0%	2.72	6313	6.43	0.16	0.10	1.26	0.54	2.58	1.84	2.54
	TW3-222	1052	4.47	19.6	7.43	807	0.96	83	1.58	1.8%	2.13	2656	6.30	0.13	0.06	1.13	0.50	2.64	1.97	2.00
	TW3-223	1075	5.21	18.8	7.50	805	1.10	94	1.38	1.6%	1.92	2037	6.43	0.13	0.05	1.07	0.53	2.63	1.99	1.89
	TW3-224	1169	8.58	18.2	7.85	803	0.98	34	0.80	0.9%	1.54	736	6.49	0.12	0.03	0.98	0.49	2.63	2.08	1.57
	TW3-225	1265	12.05	16.2	8.00	801	1.17	52	0.64	0.7%	1.40	467	6.37	0.12	0.04	0.95	0.48	2.65	2.11	1.41
late extraction	TW3-226	1440	18.82	18.0	8.14	803	1.36	35	0.46	0.5%	1.25	303	6.49	0.13	0.03	0.90	0.47	2.66	2.17	1.35
	TW3-227	1675	24.50	19.7	8.24	802	1.14	NA	0.35	0.4%	1.16	225	6.51	0.10	0.03	0.91	0.47	2.64	2.15	1.22
	EPA secondary MCL				6.5-8.5	780*												7.05	2.60	

* estimated based on the secondary MCL of 500 mg/L for TDS.

experiment stage	sample ID	Li μM	Be nM	Cr nM	Mn μM	Fe μM	Co nM	Ni μM	Cu μM	Zn μM	As nM	Se nM	Rb nM	Sr μM	Zr nM	Mo nM	Cd nM	Sb nM	Cs nM	Ba nM	Tl nM	Pb nM	U nM
background	TW3-202	5.3	1	3.9	0.01	0.11	6.8	0.04	0.02	0.8	11	<2.5	27	6	0.8	25	0.6	0.3	1.3	159	0.0	0.6	29.5
	TW3-203	5.4	1	2.9	0.01	0.41	7.5	0.08	0.02	0.8	10	<2.5	27	5	0.4	25	0.5	0.4	1.2	161	0.0	0.5	29.4
	TW3-204	5.5	1	2.7	0.01	0.06	7.4	0.10	0.03	0.9	9	<2.5	26	6	0.6	25	0.5	0.2	1.2	154	0.0	0.2	29.5
in tank	tank-1	5.0	1	4.3	0.01	0.18	7.1	0.06	0.05	0.9	8	<2.5	52	6	1.4	26	0.6	0.3	9.0	164	0.0	5.3	30.9
	tank-2	4.9	1	3.9	0.01	0.09	6.9	0.16	0.04	0.8	9	<2.5	52	6	0.6	26	0.9	0.3	5.0	185	0.0	1.5	28.8
	tank-3	5.2	1	3.9	0.01	0.19	6.8	0.06	0.04	0.8	10	<2.5	48	5	0.7	26	0.7	0.2	2.3	176	0.0	0.9	28.2
injection	TW3-205	5.4	1	3.6	0.10	1.57	7.2	0.17	0.06	1.2	9	<2.5	42	5	0.7	25	27.8	0.2	1.2	174	0.0	2.5	27.0
	TW3-206	5.6	1	3.7	0.06	1.53	6.5	0.10	0.06	1.2	11	<2.5	43	6	0.4	25	13.6	0.2	1.2	170	0.0	2.6	26.9
	TW3-207	5.6	1	4.3	0.09	2.64	6.3	0.07	0.10	1.2	9	<2.5	41	5	0.5	25	18.7	0.4	1.2	161	0.0	2.1	25.2
	TW3-208	5.9	1	2.8	0.06	2.58	6.6	0.06	0.09	2.9	10	<2.5	39	6	0.6	25	11.5	0.3	1.2	147	0.0	1.0	26.8
incubation (test sampling)	TW3-209	4.4	4	1.5	6.92	0.04	32.2	0.35	0.02	129.8	0	<2.5	57	6	0.4	24	4.4	0.6	1.0	197	0.0	0.2	20.5
	TW3-210	5.1	11	4.1	2.61	0.09	16.1	0.25	0.04	63.6	2	<2.5	67	10	0.4	28	3.9	0.5	1.3	306	0.0	0.3	44.0
early extraction	TW3-211	7.2	93	15.9	1.65	16.58	15.0	0.18	0.09	43.4	7	<2.5	110	20	4.9	24	1.6	0.3	2.3	785	0.0	0.7	114.8
	TW3-212	7.4	121	8.4	1.09	3.87	11.6	0.10	0.58	28.7	9	<2.5	107	21	6.6	12	1.8	0.2	2.3	805	0.0	0.8	94.6
	TW3-213	7.2	111	7.0	0.92	2.92	11.2	0.20	0.78	23.6	8	<2.5	102	20	7.0	11	1.6	0.4	2.1	739	0.0	0.9	90.6
	TW3-214	6.9	95	7.2	0.86	1.98	10.7	0.09	0.79	18.3	8	<2.5	97	20	5.9	10	1.2	0.3	2.1	718	0.0	0.5	84.7
	TW3-215	6.8	81	5.2	0.76	1.39	10.3	0.08	0.75	14.8	7	<2.5	90	19	5.4	10	1.1	0.3	2.1	657	0.0	0.4	81.7
	TW3-216	6.3	49	3.8	0.51	0.61	10.4	0.08	0.56	8.7	6	<2.5	72	16	3.8	11	0.8	0.3	1.8	501	0.0	0.4	75.9
	TW3-217	5.9	25	3.3	0.35	0.47	7.1	0.18	2.13		5	<2.5	59	12	1.4	15	0.7	0.3	1.6	351	0.0	1.0	67.8
	TW3-218	5.7	20		0.85		43.6	2.03	0.32		6	<2.5	52	11	1.2		0.8	0.3	1.6	312	0.1	0.6	63.7
	TW3-219	5.6	16	3.2	0.28	0.24	7.2	0.10	0.21	3.2	5	<2.5	50	11	1.0	16	0.6	0.4	1.5	304	0.0	0.5	60.3
	TW3-220	5.5	8	2.7	0.19	0.26	8.0	0.14	0.15	2.1	7	<2.5	39	8	0.9	19	0.5	0.3	1.4	217	0.0	0.5	51.6
mid extraction	TW3-221	5.6	8	3.1	0.20	0.31	23.6	1.00	0.21	1.9	7	<2.5	38	9	1.1	19	0.5	0.3	1.5	219	0.0	0.8	48.6
	TW3-222	5.9	6	2.9	0.14	0.18	6.1	0.10	0.08	1.3	8	<2.5	30	7	0.7	21	0.5	0.3	1.4	184	0.0	0.7	46.7
	TW3-223	5.9	5	3.4	0.14	0.22	6.3	0.07	0.09	8	<2.5	29	7	0.9	23	0.4	0.2	1.3	177	0.0	0.3	44.3	
	TW3-224	5.9	3		0.09	0.17																	

end of the injection experiments and significant correlations with CO_2 mixing ratios ($R=0.90$ in both injections).

Cl^- and Na concentrations did not show apparent changes during both injections. K is not discussed because KBr was added as a tracer and the mixing effect largely exceeded the changes due to geochemical reactions.

3.5. Trace elements

After CO_2 was added to the aquifer water in 2011, concentrations of trace elements, including Cr , Fe , Ni , Cu , Rb , Cd , Sb , Tl , Pb , and U , in the water samples collected during injection increased (Table 2) compared to the background aquifer water ($p < 0.1$). In 2012, after CO_2 was added, concentrations of Cu , Rb , Cd , Cs and Pb in the aquifer water stored in polyethylene storage tanks increased significantly (Table 3) compared to the background aquifer water ($p < 0.1$), which suggests possible contamination of these elements from the storage tanks. Concentrations of Li , Mn , Fe , Cu , Zn , and Cd in the injected water increased compared to the CO_2 -treated water in the storage tank ($p < 0.1$), which suggests possible contamination of these elements from the injection pump and/or injection lines. It is worth noting that minor effects of enhanced dissolution of suspended particles in the aquifer water due to CO_2 introduction and hence pH change cannot be completely excluded.

After incubation in the aquifer, the first few samples (TW3-106 to TW3-111) collected during early extraction phase showed significant differences ($p < 0.05$ in all comparisons) including 2-fold or more increased concentrations of Be , Co , Ni , Cu , Rb , Sr , Zr , Sb , Ba , and U , and up to 50 fold increases in Mn , Fe , and Zn (Fig. 2A) compared to the concentrations in the injected water in the 2011 experiment. This suggests an enhanced release of these elements under acidic (pH 6.0–6.4) and/or reducing conditions (DO decreased to below detection limit and ORP dropped to -266 mV). As and Mo concentrations decreased up to 60%, which might be due to the enhanced adsorption under lower pH conditions.

During mid-extraction phase, trace element concentrations of Be , Cr , Co , Ni , Sr , Zr , Mo , Cd , Sb and Pb were reduced to the background levels as the mixing ratio of injected CO_2 decreased to below 10% ($p > 0.05$). Concentrations of Fe , Cu , Zn , As , Rb , Ba and U were recovered to the background levels during the late extraction phase when the mixing ratio of injected CO_2 decreased to below 1% ($p > 0.05$). Mn showed significantly higher concentrations than in the background water ($p = 0.03$) and significant correlations with CO_2 mixing ratios ($R = 0.93$) toward the end of the injection experiment.

Elements such as Li , Se , Cs , and Tl did not show significant change in concentration, indicating very low mobility of these elements in the aquifer rocks.

After injection and incubation in the subsurface, similar concentration changes in the 2012 experiment were observed for trace elements (Fig. 3B) as for those in the 2011 experiment.

4. Discussion

4.1. Mechanisms of mineral dissolution and trace element release

The total CO_2 ($t\text{CO}_2 = [\text{H}_2\text{CO}_3] + [\text{HCO}_3^-] + [\text{CO}_3^{2-}]$) was also plotted (Fig. 1) and compared with the tracers. In 2011, the mass recovery percentages were 64% estimated from bromide and 71% from SF_6 , while 83% from $t\text{CO}_2$; in 2012, the bromide recovery percentage was 78% while 89% from $t\text{CO}_2$. These suggest an additional 15–30% source of carbon species, which is probably from the dissolution of carbonate minerals from the aquifer rocks due to the pH change caused by CO_2 injection, as the logarithmical $p\text{CO}_2$ in

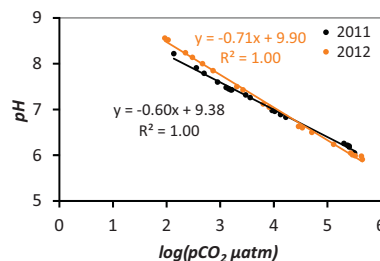


Fig. 4. Correlation between pH and $\log(p\text{CO}_2)$ in aquifer water samples during 2011 and 2012 push-pull experiments in TW-3 well.

the aquifer is strongly linearly correlated with pH in both 2011 and 2012 experiments (Fig. 4).

Mg and alkalinity showed very strong correlations ($R > 0.90$) with Ca attributable to the co-dissolution from carbonate minerals, such as calcite and dolomite. Si strongly correlated with these carbonate species, but their correlation coefficients were slightly lower, suggesting the dissolution of some silicate minerals, such as feldspars and illite. The relative abundances of SiO_2 and alkalinity in the water samples collected during extraction phases (Fig. 5) showed that the background water was dominated by silicate weathering as the alkalinity/ SiO_2 was < 5 (Hounslow, 1995), while at the early extraction phase the dissolution of carbonate minerals dominated as indicated by an alkalinity/ SiO_2 ratio > 10 despite the very high content of silica in the aquifer material (Table 1). This high degree of influence of carbonate minerals was also observed in the predominantly siliciclastic Dockum aquifer in the SACROC CO_2 -enhanced oil field in Texas (Romanak et al., 2012).

Sulfate concentrations decreased in the early extraction phase when the mixing ratio of injected CO_2 was high ($> 10\%$), and showed a strong correlation with ORP ($R = 0.72$) in the 2011 experiment, which suggests sulfate reduction occurred after CO_2 injection. The decrease of sulfate concentration in the 2012 experiment was not as dramatic as in the 2011 injection, probably due to the overall higher redox potential in the 2012 experiment. However, sulfate concentrations showed a decrease by 30% in the first two samples collected in the early extraction phase when the ORP was at a low value of 43 mV.

Alkaline earth elements Be , Rb , Sr , and Ba showed very strong correlations ($R > 0.90$) with Ca and Mg , indicating their mobilization from cation exchange reactions was triggered by the dissolution of carbonates (Trautz et al., 2013; Yang et al., 2013). Fe and Cr concentrations increased substantially after incubation in the aquifer despite the possible contamination from storage tanks and/or injection lines, and showed strong correlation in both 2011 and 2012 experiments, which is attributed to the enhanced reductive

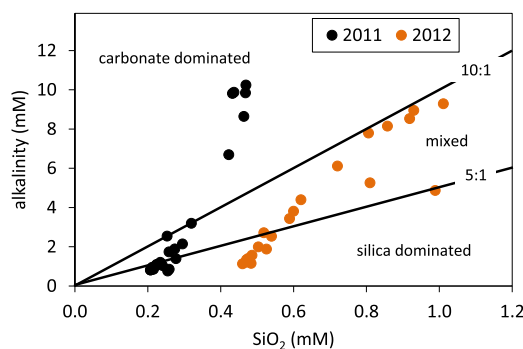


Fig. 5. The relative influence of carbonate and silicate geochemistry in the TW-3 push-pull experiments.

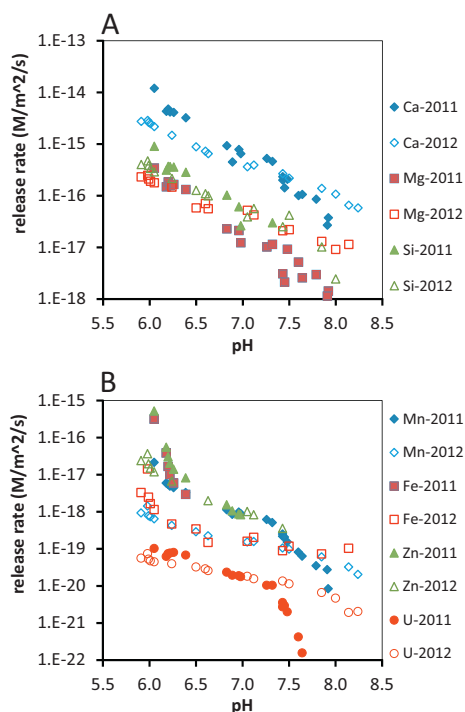


Fig. 6. Release rates of major (top) and trace elements (bottom) plotted against pH during 2011 (solid symbol) and 2012 (open symbol) push–pull experiments in TW-3 well. *Release rates are calculated using the method described in Section 2.6.

dissolution and the favored desorption of dominant Cr(III) under low pH and organic rich reducing conditions associated with CO_2 introduction into the subsurface (Richard and Bourg, 1991; Roden and Zachara, 1996). These mechanisms also contribute to the increased concentration of other transition elements, such as Mn, Co, Ni, Cu, Zn, and Zr. The mobilization of U is mainly contributed by the enhanced desorption due to the formation of uranyl carbonate complexes (Wu et al., 2006) under high CO_2 conditions. More oxic conditions in the aquifer also enhance the U mobility in groundwater by forming $\text{UO}_2^{2+}-\text{CO}_3^{2-}$ complex, while reducing aquifer conditions might reduce U(VI) to U(IV) as UO_2 , which has very low solubility in groundwater. The decrease of Mo concentrations in groundwater after CO_2 injection might be due to its binding with organic matter (Wichard et al., 2009) and enhanced adsorption under low pH environments (Goldberg and Forster, 1998).

It should be pointed out that, during the 2011 and 2012 experiments, 10–60 nM of Cd and up to 60 nM of Pb, potentially from contamination of polyethylene storage tanks and/or injection pump lines, was inadvertently injected into the aquifer (Tables 2 and 3). High Pb and Cd concentrations in the injected solution might to a certain extent suppress reactions, e.g. desorption, that could release them from aquifer materials to groundwater. The concentrations of these elements, however, were quickly reduced to near the background levels by the end of early extraction phase. This may be attributed to the scavenging by surface active organic matter (Strawn and Sparks, 2000).

4.2. Elemental release rates

The release rates of major cations including Ca, Mg and Si are comparable with those measured in batch reactors (Pokrovsky et al., 2005) and show strong linear dependence on pH (Matter et al., 2007; Pokrovsky et al., 2005) during both 2011 and 2012 experiments ($R^2 > 0.92$ for all three elements) (Fig. 6A). The release rates of Ca are 1–2 orders of magnitude higher than those of Mg and Si,

which suggests a fast and more ready dissolution of carbonate minerals than silicates. Low levels of carbonate minerals in an aquifer (~1% in this study) may contribute to significant changes of groundwater geochemistry under elevated CO_2 conditions (Romanak et al., 2012).

The release rates of trace elements, e.g. Fe, Mn, Zn and U, also showed an overall pH dependence ($R^2 > 0.73$), with higher release rates under more acidic conditions (Fig. 6B). This pH dependence is altered by the changing redox conditions in the aquifer, however. The release rates of these elements in the 2012 experiment were linearly correlated with pH ($0.94 < R^2 < 0.97$ except 0.73 for Fe), while in the 2011 experiment, the release rates of Mn, Fe and Zn were faster in the first few samples collected during the early extraction phase and showed less linearity ($0.83 < R^2 < 0.94$) (Fig. 6B). In particular, the aquifer was more reducing (DO 0–0.15 mg/L and ORP –266 to –58 mV in the 2011 experiment, compared to DO 0.13–1.36 mg/L and ORP 70–149 mV in the 2012 experiment) which enhanced the metal reduction. U did not show this change in release rate in the early extraction phase of the 2011 experiment, which can be explained by no apparent enhanced release under reducing condition in the first few samples. Furthermore, the release rate of U was inhibited in the late extraction phase of the 2011 experiment because of more reducing conditions (ORP –44 to 28 mV) than those in the 2012 experiment (ORP 34–94 mV). Besides the higher redox potential, higher carbonate concentrations in the 2012 experiment (Tables 2 and 3) may also contribute to the overall higher U concentrations in the aquifer water than in the 2011 experiment due to the complexation of UO_2^{2+} with carbonate which enhances the U mobility in the groundwater (Yang et al., 2014).

The logarithmic release rates of these major and trace elements are correlated with $\log(p\text{CO}_2)$ because of the strong linearity between $\log(p\text{CO}_2)$ and pH (Fig. 4). Thus the release rates and concentrations of major and trace elements in CO_2 geosequestration experiments may be estimated based on the spatial and temporal extent of dissolved CO_2 and aquifer characteristics. To minimize the risk of losing injected solution and thus allow a longer incubation period, only approximately 3 m³ of aquifer water mixed with 1-atm $p\text{CO}_2$ was injected. The in situ rates of elemental release, mineral dissolution, and chemical composition change of aquifer water can be estimated by extrapolation from the correlation of reaction rate to $p\text{CO}_2$ concentration. An injection of a larger volume of water, or water mixed with a higher concentration of $p\text{CO}_2$, e.g. 5-atm, can therefore be extrapolated from that correlation to higher $p\text{CO}_2$ conditions.

4.3. Extent of impact zone

In a groundwater aquifer, the spatial extent of impact zone from CO_2 leakage depends not only on the movement of CO_2 plume, which is determined by the rate and duration of CO_2 leakage and the permeability of aquifer and its surrounding rocks, but also on the hydrogeochemical conditions of aquifer sediment and fractured surfaces for bedrock aquifers that change water chemistry. In this research, the geochemical conservative tracers (bromide and SF_6) are used to quantify the CO_2 plume and movement under controlled CO_2 injection experiments in the complicated fractured bedrock aquifer with an apparent dual-porosity system. A mixing ratio of 1% injected solution based on tracer data is used as the cutoff value to define the groundwater zone affected by elevated CO_2 concentrations for the purpose of calculating the extent of the affected aquifer zone. This corresponds to the time point when approximately 10-time volume of injected solution was extracted during the pull phase, and groundwater pH, specific conductance, total CO_2 , $p\text{CO}_2$, Ca, alkalinity, and trace elements such as Mn, Rb, Sr and

U showed statistically significantly higher concentrations than the background levels.

The volume of affected aquifer water is thus estimated based on tracer data and the consideration of their recovery percentages (averaged as 71%) as 44 m^3 ($=10 \times 3.1/0.71$). We use an effective porosity of 2–5% based on borehole geophysical measurements (Burgdorff and Goldberg, 2001) and assume a cylindrical flow field around the injection well (Matter et al., 2007). We then calculate the radial distance in the ~ 2 cm thick permeable (fractured) zone to be 25–80 m. As a comparison, the radial distance of the impact zone in a porous media sedimentary aquifer with an effective porosity of 20% and a thickness of 4 m (the isolated injection depth), is only 4 m. This suggests a larger impact zone if CO_2 leaked into fracture dominated rock aquifers than if a similar volume leaked into a porous sedimentary aquifer under similar conditions. As a comparison, the reactive surface area in porous media is 300–700 times of that in fractured systems, therefore the concentrations of reactive elements could be hundreds of times higher in a porous sedimentary aquifer than in a fractured system, given a similar concentration, volume, and duration of CO_2 leakage.

Comparison of the hydrogeochemistry of background aquifer water before CO_2 injection reveals distinctly higher pH, alkalinity, Si, Li, Ba and U, and lower Mg, Ca, Cl^- , SO_4^{2-} , Rb and Sr in the 2012 experiment than in the 2011 experiment ($p < 0.05$ for all elements except 0.09 for alkalinity). This may be attributed to different groundwater sources. Although the 2011 push–pull experiment extracted a large volume of water ($\sim 120 \text{ m}^3$, or 40 times of injection volume), we cannot exclude the possibility that aquifer conditions were altered to some extent by low levels of residual CO_2 from the experiment. The recovered volume percentages of conservative tracers during the push–pull experiments were 64–78%. The residual CO_2 may contribute to the higher alkalinity and higher Si levels from silicate mineral dissolution in the 2012 experiment, as well as the release of Ba and U due to their enhanced solubility under higher alkalinity condition. The lower specific conductance, alkaline earth elements including Mg, Ca, Sr, and most of others in 2012 background water might be due to the depletion of these elements in the reactive regimes in fractures and pore space after 2011 experiment.

The hydraulically conductive zones in this sedimentary rock formation and the overlying intrusive Palisades dolerite sill are generally narrow and vertically localized (1–3 m thick). The Palisades dolerite sill and low-permeability sedimentary formations separating the conductive zones during these experiments exhibit near-zero transmissivity and thus could serve as effective caprock formations for CO_2 geological storage.

4.4. Implications for risk assessment of CO_2 geosequestration sites

Under a hypothetical CO_2 leakage scenario, the groundwater hydrochemical parameters should change significantly, including decreased pH due to enhanced CO_2 , as well as increased specific conductance and total dissolved solid (TDS) due to mineral and trace element dissolution. Major elements including Ca, Mg, Si and alkalinity, and trace elements including Mn, Fe, Cr, Co, Ni, Cu, Zn, Rb, Sr, Ba, and U increased in concentration by up to 100-fold due to the increased acidity and altered redox conditions in the aquifer. Sulfate concentrations showed a slight decrease, probably due to the microbial sulfate reduction. The concentration change in these elements may be sensitive indicators of CO_2 leakage at geosequestration sites. We conclude from this study that close geochemical monitoring of groundwater aquifers should be used to detect the potential leakage or upwelling from deeper CO_2 injection reservoirs. In particular, parameters including pH, alkalinity, Ca (Romanak et al., 2012; Trautz et al., 2013), $p\text{CO}_2$, Mn and U showed statistically significant concentration difference from the

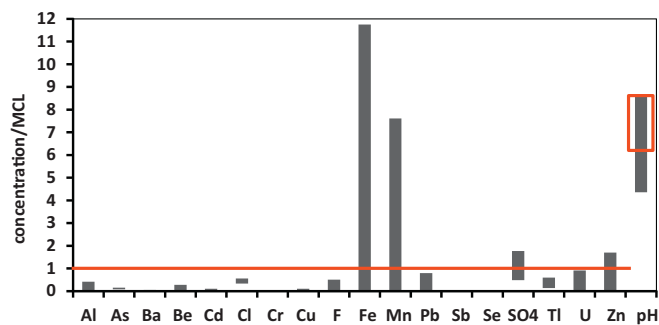


Fig. 7. Concentration ranges of ions and pH during 2011 and 2012 push–pull experiments in TW-3 well. *For better illustration, concentrations normalized by the U.S. EPA drinking water Maximum Contaminant Levels as highlighted in red. (For interpretation of the references to color in this figure legend, the reader is referred to the web version of the article.)

background levels ($p \leq 0.1$) when the mixing ratio of the injected groundwater was only 1%, or the $p\text{CO}_2$ was only $\sim 2000 \mu\text{atm}$. These parameters may be used as sensitive indicators of the CO_2 plume front or even small quantities of CO_2 leakage.

Public and private wells tap into various groundwater aquifers above potential saline reservoirs proposed for geosequestration, making it very important to understand the potential risks to drinking water resources associated with CO_2 injection. Compared to the primary drinking water Maximum Contaminant Levels (MCLs), no inorganic chemicals levels measured in this research exceeded these regulations. However, elemental levels were above the secondary drinking water MCLs in pH, Fe, Mn, and Zn (Fig. 7, Tables 2 and 3), indicating that CO_2 leakage after injection may cause hydrogeochemical parameters to exceed regulations. The interval of the Newark Basin sediments studied in this research has relatively low concentrations of fine grained minerals and trace metals, however, and our injection experiments utilized very low $p\text{CO}_2$ concentrations. Other aquifers in different formation lithologies or injection of more acidic, higher $p\text{CO}_2$ conditions may result in enhanced concentrations of other major or trace elements that exceed the MCL regulations.

5. Conclusions

This study presented two single-well push–pull injection tests in a fracture zone of freshwater bedrock aquifer in the Newark Basin to quantify the hydrogeochemical processes and element release and assess the potential impacts on the shallow groundwater quality in response to CO_2 leakage. Conservative tracers of bromide and SF_6 were used to quantify the mixing processes and transport of injected CO_2 and suggested a dual-porosity system in the aquifer.

Following the injection of aquifer water enhanced with 1 atm $p\text{CO}_2$ and incubation for 3–6 weeks in the sand and clay formation, results of groundwater analysis showed a decrease of pH by 2–3, a depletion of dissolved oxygen and a sharp drop of redox potential, and an increase of specific conductance. Major cation concentrations increased significantly to 3.0–5.2 times of background levels for Ca, 1.8–3.5 times for Mg, and 1.8–2.1 times for Si, alkalinity increased dramatically to 7.9–11.9 times, while sulfate concentrations decreased by 20–30%. Trace elements showed 2-fold or more increased concentrations of Be, Cr, Co, Ni, Cu, Rb, Sr, Zr, Sb, Ba and U, up to 50-fold increase in Mn, Fe and Zn, and a decreased concentration of As and Mo. These hydrogeochemical parameters and elemental concentrations returned to the background levels toward the end of the extraction phase. Elevated levels of Pb and Cd (10–50 times above the background levels) were injected inadvertently to the aquifer, and were found to be reduced to the background levels within about 200 h.

Mobilization of major cations and alkalinity were attributed to the enhanced dissolution of carbonate and silicate minerals under elevated $p\text{CO}_2$ condition in the subsurface. The release rates of Ca, Mg and Si are comparable with those from batch experiments and show strong dependence on pH and $p\text{CO}_2$. Carbonate dissolution contributed to significant change of water geochemistry even though its content in the aquifer material might be low ($\sim 1\%$). The decrease of pH and reducing condition followed CO_2 injection enhanced mobilization of trace elements through reduction, dissolution and desorption from aquifer minerals, and complexation with carbonate/bicarbonate.

An altered background condition in the aquifer after the first injection was observed. This suggests an introduction of different water source into the study zone and/or a change in aquifer condition to low levels of residual CO_2 . Considering the low transmissivity, a larger impact zone can be expected if CO_2 leaked into fracture dominated rock aquifers than in porous sedimentary aquifers under similar leakage conditions.

Rapid and simultaneous changes of pH, specific conductance, major and trace element release in aquifer water could be used as monitoring indicators of CO_2 leakage from geologic sequestration sites. pH, Ca, and Mn showed significant difference from background levels under very low $p\text{CO}_2$ condition, thus can be used as sensitive indicators of the CO_2 plume front or even small quantities of CO_2 leakage.

Minor deterioration of shallow groundwater quality, particularly exceeding the secondary drinking water MCLs in pH, Fe, Mn and Zn, was observed under CO_2 leakage scenario. These parameters should be carefully monitored to assure compliance with the U.S. EPA drinking water regulations.

Acknowledgements

This research is financially supported by the U.S. Environmental Protection Agency STAR Grant # 834503. Walter Masterson of LDEO provided technical support during field work. The authors also thank Alan Seltzer of Columbia University for assistance in laboratory and field work. This is LDEO contribution # 7782.

References

- Assayag, N., Matter, J., Ader, M., Goldberg, D., Agrinier, P., 2009. Water–rock interactions during a CO_2 injection field-test: implications on host rock dissolution and alteration effects. *Chem. Geol.* 265, 227–235.
- Bachu, S., 2008. CO_2 storage in geological media: role, means, status and barriers to deployment. *Prog. Energy Combust. Sci.* 34, 254–273.
- Burgdorff, K., Goldberg, D., 2001. Petrophysical characterization and natural fracturing in an olivine-dolerite aquifer. *Vis. Geosci.* 6, 1–28.
- Cheng, Z., Zheng, Y., Mortlock, R., van Geen, A., 2004. Rapid multi-element analysis of groundwater by high-resolution inductively coupled plasma mass spectrometry. *Anal. Bioanal. Chem.* 379, 512–518.
- Chipman, D.W., Marra, J., Takahashi, T., 1993. Primary production at 47°N and 20°W in the North Atlantic Ocean: a comparison between the ^{14}C incubation method and the mixed layer carbon budget. *Deep-Sea Res. Part II: Top. Stud. Oceanogr.* 40, 151–169.
- Dickson, A.G., 2001. Reference materials for oceanic CO_2 measurements. *Oceanography* 14, 21–22.
- Goldberg, S., Forster, H.S., 1998. Factors affecting molybdenum adsorption by soils and minerals. *Soil Sci.* 163, 109–114.
- Hounslow, A.W., 1995. *Water Quality Data: Analysis and Interpretation*. Lewis Publishers, New York.
- Icenhower, J.P., Saldi, G.D., Knauss, K.G., 2013. Contrasts in the geochemical behavior of carbonate and siliciclastic rocks during carbon storage and sequestration. In: *Proceedings of the Fourteenth International Symposium on Water–Rock Interaction, WRI 14*, Elsevier Science BV, Amsterdam.
- IPCC, 2005. In: Metz, B., Davidson, O., de Coninck, H., Loos, M., Meyer, L. (Eds.), *Carbon Dioxide Capture and Storage*. Cambridge University Press, UK, p. 431.
- Keating, E., Fessenden, J., Kanjorski, N., Koning, D., Pawar, R., 2010. The impact of CO_2 on shallow groundwater chemistry: observations at a natural analog site and implications for carbon sequestration. *Environ. Earth Sci.* 60, 521–536.
- Keating, E.H., Newell, D.L., Viswanathan, H., Carey, J.W., Zylvoloski, G., Pawar, R., 2013. CO_2 /brine transport into shallow aquifers along fault zones. *Environ. Sci. Technol.* 47, 290–297.
- Kharaka, Y.K., Thordsen, J.J., Hovorka, S.D., Seay Nance, H., Cole, D.R., Phelps, T.J., Knauss, K.G., 2009. Potential environmental issues of CO_2 storage in deep saline aquifers: geochemical results from the Frio-I Brine Pilot test, Texas, USA. *Appl. Geochem.* 24, 1106–1112.
- Kharaka, Y.K., Thordsen, J.J., Kakouros, E., Ambats, G., Herkelrath, W.N., Beers, S.R., Birkholzer, J.T., Apps, J.A., Spycher, N.F., Zheng, L.E., Trautz, R.C., Rauch, H.W., Gullickson, K.S., 2010. Changes in the chemistry of shallow groundwater related to the 2008 injection of CO_2 at the ZERT field site, Bozeman, Montana. *Environ. Earth Sci.* 60, 273–284.
- Lemieux, J.M., 2011. Review: the potential impact of underground geological storage of carbon dioxide in deep saline aquifers on shallow groundwater resources. *Hydrogeol. J.* 19, 757–778.
- Little, M.G., Jackson, R.B., 2010. Potential impacts of leakage from deep CO_2 geosequestration on overlying freshwater aquifers. *Environ. Sci. Technol.* 44, 9225–9232.
- Lu, J., Partin, J.W., Hovorka, S.D., Wong, C., 2010. Potential risks to freshwater resources as a result of leakage from CO_2 geological storage: a batch-reaction experiment. *Environ. Earth Sci.* 60, 335–348.
- Matter, J., Goldberg, D., Morin, R., Stute, M., 2006. Contact zone permeability at intrusion boundaries: new results from hydraulic testing and geophysical logging in the Newark Rift Basin, New York, USA. *Hydrogeol. J.* 14, 689–699.
- Matter, J.M., Takahashi, T., Goldberg, D., 2007. Experimental evaluation of in situ CO_2 –water–rock reactions during CO_2 injection in basaltic rocks: implications for geological CO_2 sequestration. *Geochim. Geophys. Geosyst.* 8 (2), Q02001, <http://dx.doi.org/10.1029/2006GC001427>.
- McGrail, B.P., Schaefer, H.T., Ho, A.M., Chien, Y.J., Dooley, J.J., Davidson, C.L., 2006. Potential for carbon dioxide sequestration in flood basalts. *J. Geophys. Res.: Solid Earth* 111, 13.
- Olsen, P.E., Kent, D.V., Cornet, B., Witte, W.K., Schlichte, R.W., 1996. High-resolution stratigraphy of the Newark rift basin (early Mesozoic, eastern North America). *Geol. Soc. Am. Bull.* 108, 40–77.
- Peter, A., Lamert, H., Beyer, M., Hornbruch, G., Heinrich, B., Schulz, A., Geistlinger, H., Schreiber, B., Dietrich, P., Werban, U., Vogt, C., Richnow, H.-H., Grobmann, J., Dahmke, A., 2012. Investigation of the geochemical impact of CO_2 on shallow groundwater: design and implementation of a CO_2 injection test in Northeast Germany. *Environ. Earth Sci.* 67, 335–349.
- Pokrovsky, O.S., Golubev, S.V., Schott, J., 2005. Dissolution kinetics of calcite, dolomite and magnesite at 25 C and 0 to 50 atm $p\text{CO}_2$. *Chem. Geol.* 217, 239–255.
- Richard, F.C., Bourg, A.C.M., 1991. Aqueous geochemistry of chromium: a review. *Water Res.* 25, 807–816.
- Roden, E.E., Zachara, J.M., 1996. Microbial reduction of crystalline iron(III) oxides: influence of oxide surface area and potential for cell growth. *Environ. Sci. Technol.* 30, 1618–1628.
- Romanak, K.D., Smyth, R.C., Yang, C., Hovorka, S.D., Rearick, M., Lu, J., 2012. Sensitivity of groundwater systems to CO_2 : application of a site-specific analysis of carbonate monitoring parameters at the SACROC CO_2 -enhanced oil field. *Int. J. Greenhouse Gas Control* 6, 142–152.
- Rosen, O.M., Abayazov, A.A., Tipper, J.C., 2004. MINLITH—an experience-based algorithm for estimating the likely mineralogical compositions of sedimentary rocks from bulk chemical analyses. *Comput. Geosci.* 30, 647–661.
- Strawn, D.G., Sparks, D.L., 2000. Effects of soil organic matter on the kinetics and mechanisms of Pb(II) sorption and desorption in soil. *Soil Sci. Soc. Am. J.* 64, 144–156.
- Trautz, R.C., Pugh, J.D., Varadarajan, C., Zheng, L., Bianchi, M., Nico, P.S., Spycher, N.F., Newell, D.L., Esposito, R.A., Wu, Y., Dafflon, B., Hubbard, S.S., Birkholzer, J.T., 2013. Effect of dissolved CO_2 on a shallow groundwater system: a controlled release field experiment. *Environ. Sci. Technol.* 47, 298–305.
- Wichard, T., Mishra, B., Myneni, S.C.B., Bellenger, J.P., Kraepiel, A.M.L., 2009. Storage and bioavailability of molybdenum in soils increased by organic matter complexation. *Nat. Geosci.* 2, 625–629.
- Wu, W.M., Carley, J., Gentry, T., Ginder-Vogel, M.A., Fienen, M., Mehlhorn, T., Yan, H., Carroll, S., Pace, M.N., Nyman, J., Luo, J., Gentile, M.E., Fields, M.W., Hickey, R.F., Gu, B.H., Watson, D., Cirpka, O.A., Zhou, J.Z., Fendorf, S., Kitanidis, P.K., Jardine, P.M., Criddle, C.S., 2006. Pilot-scale in situ bioremediation of uranium in a highly contaminated aquifer. 2. Reduction of U(VI) and geochemical control of U(VI) bioavailability. *Environ. Sci. Technol.* 40, 3986–3995.
- Yang, C., Mickler, P.J., Reedy, R., Scanlon, B.R., Romanak, K.D., Nicot, J.-P., Hovorka, S.D., Trevino, R.H., Larson, T., 2013. Single-well push–pull test for assessing potential impacts of CO_2 leakage on groundwater quality in a shallow Gulf Coast aquifer in Cranfield, Mississippi. *Int. J. Greenhouse Gas Control* 18, 375–387.
- Yang, Q., Smitherman, P., Hess, C.T., Culbertson, C.W., Marvinney, R.G., Smith, A.E., Zheng, Y., 2014. Uranium and radon in private bedrock well water in Maine: geospatial analysis at two scales. *Environ. Sci. Technol.* 48, 4298–4306.
- Zheng, L., Apps, J.A., Spycher, N., Birkholzer, J.T., Kharaka, Y.K., Thordsen, J., Beers, S.R., Herkelrath, W.N., Kakouros, E., Trautz, R.C., 2012. Geochemical modeling of changes in shallow groundwater chemistry observed during the MSU-ZERT CO_2 injection experiment. *Int. J. Greenhouse Gas Control* 7, 202–217.